J Mater Sci (2007) 42:4716–4719
DOI 10.1007/s10853-007-1758-8

LETTER

SEM-ECC observations of dislocation structures in a cyclically deformed Cu single crystal oriented for [$\bar{2}$23] conjugate double slip

Xiao-Wu Li · Yang Zhou

Received: 5 March 2007 / Accepted: 9 April 2007 / Published online: 16 May 2007

Dislocation structures induced by the cyclic deformation of single-slip-oriented Cu single crystals have been extensively investigated mainly by transmission electron microscope (TEM) and well-documented in the last four decades [1–3]. It is recognized that the dislocation structures of fatigued Cu single crystals oriented for single slip are strongly dependent upon the applied plastic strain amplitude γ_{pl}, and that the well-known two-phase structure of persistent slip band (PSB) ladders and matrix veins forms in the range of γ_{pl} corresponding to the plateau region in the cyclic stress-strain (CSS) curve of the crystal [4, 5]. However, double- and/or multiple-slip are frequently seen to operate in polycrystals and it may thus not be appropriate to relate simply the cyclic deformation behavior of single-slip-oriented crystals to that of polycrystals. Therefore, quite recently, we investigated systematically the cyclic deformation behavior of double- and multiple-slip-oriented Cu single crystals [6–12]. A comprehensive knowledge of the dislocation microstructures in cyclically deformed Cu single crystals with various orientations is still limited, although some efforts have been previously made [13–19]. In the present study, dislocation structures in a fatigued Cu single crystal oriented for [$\bar{2}$23] conjugate double slip are examined using electron channelling contrast (ECC) technique in scanning electron microscope (SEM). By comparison with other results on the [$\bar{1}$17] crystal [19], [001] crystal [15] and [$\bar{1}$11] crystal [14, 17], an orientation dependence of dislocation structures in fatigued Cu single crystals with orientation being located on the [001]–[$\bar{1}$11] side of the standard stereographic triangle (see Fig. 1) will be revealed.

[$\bar{2}$23] single crystals were grown from OFHC copper of 99.999% purity by the Bridgman technique. The dimensions of the fatigue specimen are $7 \times 7 \times 70$ mm^3, with a gauge section of $7 \times 5 \times 16$ mm^3. The orientation of the specimen was determined by the Laue back-reflection technique with an accuracy within ±2°. Before the fatigue tests, the specimens were electro-polished to produce a strain-free and mirror-like surface for microscopic observations. Push-pull fatigue tests were performed at room temperature in air using a Shimadzu servo-hydraulic testing machine. A triangular waveform signal with a frequency range of 0.05–0.4 Hz was used for the constant plastic strain control. The plastic resolved shear strain amplitude γ_{pl} and shear stress τ are calculated by $\gamma_{pl} = \Delta\varepsilon_p/2\Omega$ and $\tau = \sigma\Omega$, where Ω is the Schmid factor of the

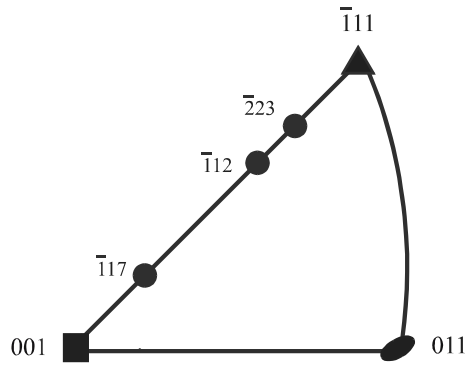

Fig. 1 Standard stereographic triangle showing the orientations of Cu single crystals involved in this paper

X.-W. Li (✉) · Y. Zhou
Institute of Materials Physics and Chemistry, College of Sciences, Northeastern University, P.O. Box: 104, No. 3-11, Wenhua Road, Heping District, Shenyang 110004, P.R. China
e-mail: xwli@mail.neu.edu.cn

X.-W. Li
Key Laboratory for Anisotropy and Texture Engineering of Materials (Ministry of Education), Northeastern University, Shenyang 110004, P.R. China

primary slip system and σ is an average value of the peak stresses in tension and compression. The crystal specimens were deformed cyclically up to the occurrence of quasi-saturation. After the fatigue tests, one of the deformed surfaces was polished mechanically and then electrolytically for observation of dislocation structures by SEM-ECC. The detailed eletro-polishing procedures and the parameters of SEM working conditions can be found in Ref. [16].

The fatigue testing conditions and data for the [$\bar{2}23$] crystal have been reported in Ref. [9]. Here, the CSS curve of the [$\bar{2}23$] crystal is reproduced in Fig. 2, where the results obtained with [$\bar{1}12$] [9], [$\bar{1}17$] [19] and [001] [20] crystals as well as that of single-slip crystals [5] are included for comparison. As is well known, the CSS curves of single-slip-oriented copper single crystals exhibit a clear plateau in the range of $6.0 \times 10^{-5} < \gamma_{pl} < 7.5 \times 10^{-3}$ [5]. The CSS curve of the [$\bar{1}12$] crystal shows a clearly shorter plateau in the range of $5.0 \times 10^{-4} < \gamma_{pl} < 4.0 \times 10^{-3}$ with an average saturation stress of 28.6 MPa, which is fairly close to the results of single-slip crystals. For the [$\bar{2}23$] crystal, when $\gamma_{pl} < 1.5 \times 10^{-3}$, the crystal just exhibits a quasi-saturation stage, and no saturation (even no quasi-saturation) stage occurred when $\gamma_{pl} > 1.5 \times 10^{-3}$ [9]. So, the CSS curve of the [$\bar{2}23$] crystal can just be roughly given in the range of $\gamma_{pl} < 1.5 \times 10^{-3}$. Apparently, its CSS curve shows a plateau region with a slightly higher saturation stress of 29.9 MPa within the strain amplitude range investigated. For [$\bar{1}17$] and [001] crystals, their CSS curves do not exhibit any plateau regions [19, 20].

The dislocation structures of the cyclically deformed [$\bar{2}23$] crystal at different plastic strain amplitudes were observed by the SEM-ECC technique. Figure 3 shows the dislocation structures formed at a lower strain amplitude γ_{pl}

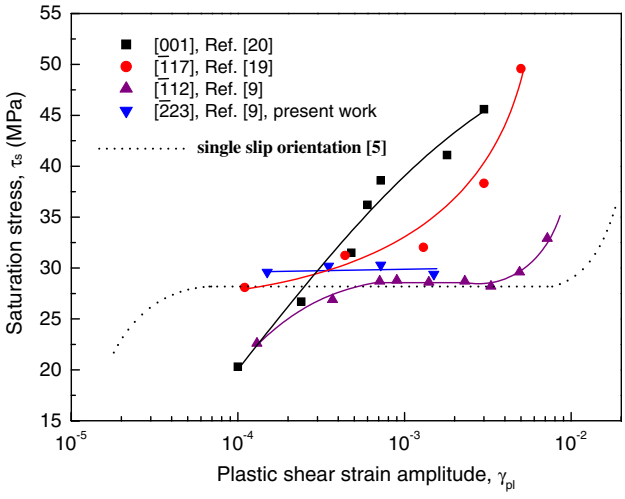

Fig. 2 The cyclic stress-strain curves of differently oriented crystals

of 1.5×10^{-4} with a cumulative plastic strain $\gamma_{pl,cum}$ of 49.2. The observed plane is ($\bar{3}\,0\,\bar{2}$). At such a low γ_{pl}, the dislocation structure consists mainly of matrix vein structures, but a few long and straight persistent slip bands (PSBs) formed along the (111) primary slip plane in some local regions, as shown in Fig. 3a. It is interesting to find that the PSBs do not show the traditional ladder patterns as often observed in the single-slip crystal. Clearly, these PSBs are composed of irregular dislocation cells, as seen in a magnified image in Fig. 3b). As γ_{pl} increases to 1.5×10^{-3} ($\gamma_{pl,cum} = 60.0$), the secondary (conjugate) slip system was found to operate, as presented in Fig. 4a, two sets of PSBs form along the primary and conjugate slip planes, respectively. The secondary (conjugate) PSBs show irregular ladder-like arrangements (see Fig. 4b), whereas the primary PSBs are well-developed and they are almost composed of relatively regular cells aligned strictly along the primary slip plane (see Fig. 4c).

Apparently, PSBs might exhibit different dislocation features depending upon the crystallographic orientation and the plastic strain amplitude imposed, as schematically shown in Fig. 5, such as regular ladder structures (Fig. 5a) often observed in single-slip crystals, irregular cell structures (Fig. 5b) observed at a low plastic strain amplitude in the present [$\bar{2}23$] double-slip crystal, or regular cell structures (Fig. 5c) formed at a comparatively high plastic strain amplitude. In fact, Lepisto et al. [21] investigated the PSB structure in [$\bar{1}11$] multiple-slip-oriented Cu single crystals by TEM and found that the PSB must not necessarily consist only of walls or ladders but they may contain also other features such as cells in fatigued [$\bar{1}11$] crystals. Since the location of the present [$\bar{2}23$] crystal in the standard triangle is quite near that of the [$\bar{1}11$] crystal, there is no doubt that the dislocation structures of both crystals show some similarities. However, it should be pointed out that the current SEM-ECC mesoscopic observations cover a much wider field of view if compared with TEM observations, as shown in Figs. 3 and 4, which embodies more convincingly and clearly the misoriented cell structure of PSBs. From Fig. 3 and 4 it can been seen that the configuration of the PSB cells changes from irregular to regular with increasing γ_{pl}. That is to say, the regular cell structure of PSBs aligned along the primary slip plane could accommodate much more plastic strains if compared with the irregular PSB cells. Such a regular cell structure of PSBs is probably related to the gradually enhanced operation of the secondary slip system in PSBs [22]. It is believed that, regardless of the PSB configurations, these PSBs should be the soft phase, which could carry the majority of the plastic strain in the course of cyclic deformation, and thus result in the occurrence of a shorter stress plateau region in the CSS curve of the present [$\bar{2}23$] crystal.

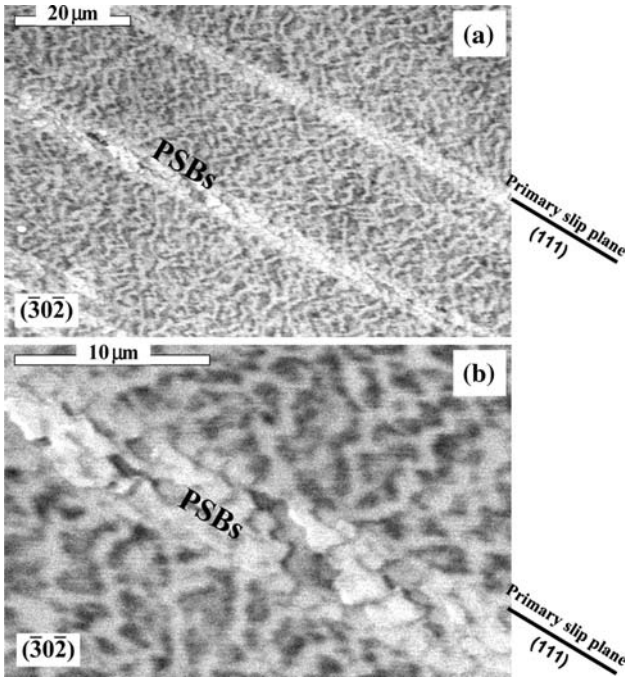

Fig. 3 SEM-ECC images of dislocation structures in the [$\bar{2}$23] crystal cycled at $\gamma_{pl} = 1.5 \times 10^{-4}$. (**a**) low magnification, and (**b**) high magnification

Besides the general slip bands and PSBs, another important deformation feature defined as deformation bands (DBs) is often seen on the surface of fatigued single crystals [23–29], especially with double or multiple slip orientations [30, 31]. Gong et al. [31] discovered that the dislocation structures of DBs consist of labyrinth and secondary PSB ladders in the [001] multiple-slip crystal. Li et al. [30] found that the dislocation structures of DBs formed in a cyclically deformed [$\bar{1}$35] single-slip crystal are composed of irregular PSB ladder structures. The present work using SEM-ECC technique demonstrates that the dislocation structures of DBs in the [$\bar{2}$23] crystal are made up of some irregular wall structures and cell structures, as shown in Fig. 6. As is well known, deformation bands resulting from deformation localization in crystals should be areas of plastic strain accumulation. When the imposed cumulative strain carried by the preferably formed DBs reaches a certain capacity, the microstructures in these DBs may transform from a certain structure (e.g., PSB ladder structure) into more stable structures (e.g., walls or cells). For differently oriented crystals cycled at different plastic strain amplitudes, the dislocation structure relevant to DBs might thus correspond to different structures that

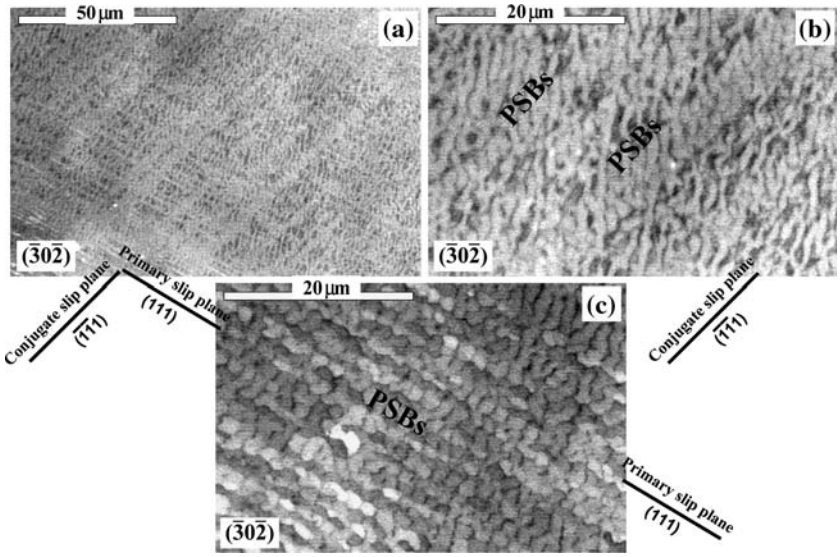

Fig. 4 SEM-ECC images of dislocation structures in the [$\bar{2}$23] crystal cycled at $\gamma_{pl} = 1.5 \times 10^{-3}$. (**a**) two slip systems operated in the crystal, (**b**) irregular PSBs along the conjugate slip plane, and (c) PSB cell structures along the primary slip plane

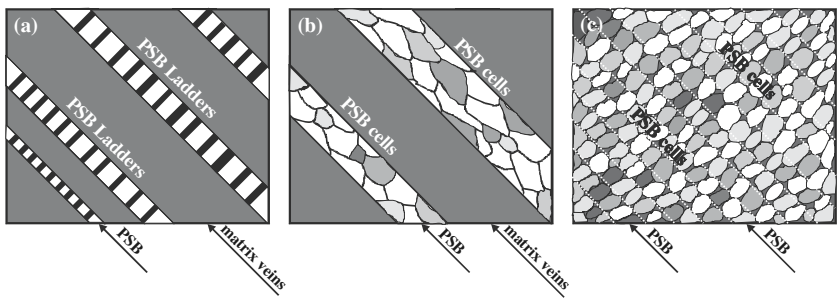

Fig. 5 Schematics of different dislocation structures of PSBs. (**a**) regular ladder structure often observed in single-slip crystals, (**b**) irregular cell structure at a low γ_{pl} of 1.5×10^{-4} in the [$\bar{2}$23] crystal, and (**c**) regular cell structure at a high γ_{pl} of 1.5×10^{-3} in the [$\bar{2}$23] crystal

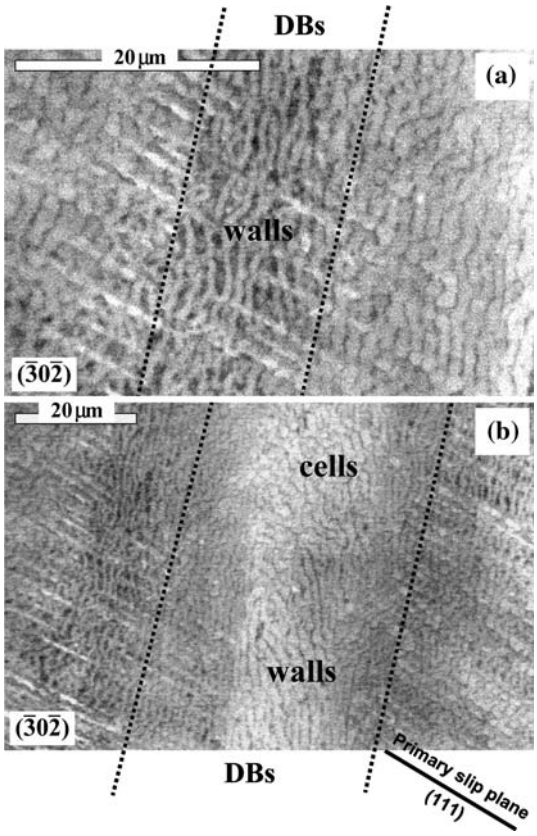

Fig. 6 SEM-ECC image of dislocation structures in DBs in the [$\bar{2}$23] crystal cycled at $\gamma_{pl} = 1.5 \times 10^{-3}$. (**a**) wall structures, and (**b**) cell and wall structures

should be more favorable to carry large plastic strain. Recently, Zhang et al. [29] suggested a new model of plastic strain distribution differing from the so-called two-phase model proposed by Winter [4]. In light of their model, the plastic strain carried by DBs is much higher than that by matrix or regular slip bands, and the DBs can even dominate the deformation mode at high plastic strain amplitudes [29]. It is thus expected that such deformation bands formed in cyclic deformation would also act as a soft phase to accommodate much more plastic strain, affecting the initiation and propagation of fatigue cracks along these DBs.

In summary, for the oriented crystals located on the [001]–[$\bar{1}$11] side of the stereographic triangle, the dislocation structure changes regularly with the variation in crystallographic orientation. For example, typical PSB ladder structures form in the [$\bar{1}$12] crystal [19]. However, as the orientation goes to [$\bar{2}$23] along the [001]–[$\bar{1}$11] side, the ladder structures in PSBs in the crystal disappear gradually and the PSBs tend to consist of irregular or regular dislocation cells; for the [$\bar{1}$11] multiple-slip crystal, cell structures are prominent [17]. As the orientation turns in reverse direction to [$\bar{1}$17] along the [001]–[$\bar{1}$11] side, no PSB ladders form, and veins, labyrinths and cells are its characteristic dislocation patterns [19]. For the [001] multiple-slip crystal, labyrinth structure was found to accommodate the applied strains during cycling [15]. Such a crystallographic orientation dependence of dislocation structure is believed to be closely related with the different geometrical relationships between orientations and corresponding slip systems in the differently oriented crystals.

Acknowledgements This research was financially supported by the Scientific Research Foundation for the Returned Overseas Chinese Scholars, Northeastern University and State Education Ministry. Prof. X.W. Li is grateful for these supports. This work was also partially supported by the National Natural Science Foundation of China (NSFC) under Grant No. 50671023. Thanks are also due to Mr. H.H. Su and Dr. R.Q. Yang for assistances with regard to SEM-ECC observations.

References

1. Laird C, Charsley P, Mughrabi H (1986) Mater Sci Eng A 81: 433
2. Basinski ZS, Basinski SJ (1992) Prog Mater Sci 36:89
3. Suresh S (1998) Fatigue of materials. Cambridge University Press, London
4. Winter AT (1974) Phil Mag 30:719
5. Mughrabi H (1978) Mater Sci Eng 33:207
6. Li XW, Wang ZG, Li GY, Wu SD, Li SX (1998) Acta Mater 46:4497
7. Li XW, Wang ZG, Li SX (1999) Mater Sci Eng A 260:132
8. Li XW, Wang ZG, Li SX (1999) Mater Sci Eng A 265:18
9. Li XW, Wang ZG, Li SX (1999) Mater Sci Eng A 269:166
10. Li XW, Wang ZG, Li SX (1999) Phil Mag Lett 79:715
11. Li XW, Wang ZG, Li SX (1999) Phil Mag Lett 79:869
12. Li XW, Wang ZG, Li SX (2000) J Mater Sci Lett 19:641
13. Jin NY (1987) Phil Mag Lett 56:23
14. Lepisto TK, Kuokkala V-T, Kettunen PO (1986) Mater Sci Eng 81:457
15. Wang ZR, Gong B, Wang ZG (1997) Acta Mater 45:1379
16. Li XW, Zhang ZF, Wang ZG, Li SX, Umakoshi Y (2001) Defect Diff Forum 188–199:153
17. Li XW, Umakoshi Y, Wang ZG, Li SX (2001) Z Metallkd 92:1222
18. Li XW, Wang ZG, Zhang YW, Li SX, Umakoshi Y (2002) Phys Stat Sol (a) 191:97
19. Li XW, Umakoshi Y, Gong B, Li SX, Wang ZG (2002) Mater Sci Eng A 333:51
20. Gong B, Wang ZR, Wang ZR (1997) Acta Mater 45:1365
21. Lepisto T, Kuokkala V-T, Kettunen P (1984) Scripta Metall 18:245
22. Wang RH, Mughrabi H (1984) Mater Sci Eng 63:147
23. Gostelow CR (1971) Metal Sci J 5:177
24. Saletore M, Taggart R (1978) Mater Sci Eng 36:259
25. Jin NY, Winter AT (1984) Acta Metall 32:989
26. Jin NY (1987) Phil Mag Lett 56:23
27. Vorren O, Ryum N (1988) Acta Metall 36:1443
28. Zhai T, Martin JW, Briggs GAD, Willkinson AJ (1996) Acta Metall 44:3477
29. Zhang ZF, Wang ZG, Sun ZM (2001) Acta Mater 49:2875
30. Li XW, Li SX, Wang ZG (2000) Phil Mag A 80:1901
31. Gong B, Wang ZR, Chen DL, Wang ZG (1997) Scripta Mater 37:1605